High Temperatures–High Pressures, 1992, volume 24, pages 23–34

The application of a pseudopotential approach to the physics of binary intermetallic compounds

Uwe Walzer
Institut für Geowissenschaften, Universität Jena, Burgweg 11, 6900 Jena, Germany
Received 27 April 1990

Abstract. A pseudopotential theory has been developed further and used for intermetallic compounds and alloys. This approach is based on relativistic quantum mechanics. *l*-dependent radii and characteristic pseudopotential constants have been newly obtained by means of this theory. They, and two other dual coordinates that can be derived from them, were used to produce plots with the aid of a computer. Through the combination of the theoretical characteristic quantities, the diagrams obtained make it possible to predict the space group and structure type of as yet undiscovered or unmeasured binary compounds, and to estimate the size of the lattice constants in a simple way. Measured data from 1364 substances were used for verification.

1 Introduction

The present paper is the first of a number of publications which are designed to demonstrate how, even if only medium-capacity computers are used, a pseudopotential theory allows the practical prediction of physical properties of intermetallic compounds and alloys: melting temperature, space group of the crystal, lattice constants, etc. Empirical pseudopotentials have been used for a long time. Their parameters can be varied such that it is possible to calculate with reasonable accuracy the reflectivity and absorption spectra, band structures, or the distribution of the electronic charge density. One frequently used empirical pseudopotential is that introduced by Ashcroft (1966). The decisive implicit assumption of this potential is that the volume integral of the sum of the attractive Coulomb force and the repulsive Pauli force from the origin to the empty-core radius vanishes in the core region.

A combination of the Ashcroft pseudopotential theory and the muffin-tin orbital theory was used, for example by Walzer (1987a, 1987b), for numerically calculating for d-state metals the relative volume as a function of the static pressure or of the Hugoniot pressure, and for comparing it with experimental data. It was also possible to predict the bulk modulus and the initial pressure derivative of the bulk modulus. It is the principal advantage of the pseudopotential calculations that, in contrast to all-electron calculations, one does not have to take into consideration atomic core states, but can make do with the contribution of the electrons of the incomplete shells.

As is well known, the self-consistency of pseudopotentials is achieved as follows. The mathematical form of the pseudopotential and naturally also the number of parameters to be varied are specified, and initial parameters are chosen. Instead of the true potential, the first trial pseudopotential is substituted in the Schrödinger equation, which then is solved numerically. The pseudocharge density is obtained from the pseudo wave functions. First, the pseudocharge density is substituted in a Poisson equation, the solution of which then yields a Hartree potential. Second, the exchange and correlation term of the potential is calculated from the pseudocharge density. With model parameters being taken into account, a summation yields the total potential, which in turn is substituted in the Schrödinger equation, and so forth. In this way, it is possible, for example, to reasonably well approximate a modulated reflectivity spectrum by means of a 'theoretical' curve. The pseudopotential

parameters gained through fitting represent a practically usable data reduction, eg for the modulated reflectivity spectrum measured. The pseudopotentials thus obtained do not have a good transferability; that is, in another chemical environment they often lead to poor prediction.

A significant step forward was the introduction of first-principle pseudopotentials (Topiol et al 1977; Zunger and Cohen 1978) which were derived from the density functional formalism (Hohenberg and Kohn 1964; Kohn and Sham 1965). From them, the total energy of solids as well as structural properties can be predicted (Ihm et al 1979). On account of the well-known pseudopotential nonuniqueness, it is necessary to make a few qualifying conditions for the ab initio pseudopotentials. A number of authors impose a maximum wave-function similarity, while others use a soft-core pseudopotential, $V_{ps}^{(l)}(r)$, with $\lim_{r\to 0} V_{ps}^{(l)}(r) = \text{constant}$. This gives only an insufficient representation of those parts of the wave functions that are important for the chemical bond. The present work continues the line of development which was put forward by Hamann et al (1979). The potentials are angular momentum dependent.

The conditions made are as follows. A core radius is positioned between the outer maximum and the first zero of the all-electron wave function. Outside the core radius, the pseudo wave function and the all-electron wave function are in agreement with one another. Since this is the chemically relevant valence region, the chemical bond is thereby optimally described. A second condition concerns the agreement between the all-electron and the pseudo valence eigenvalues for a prototype atomic configuration. To ensure an optimum transferability, two further requirements are made: for radii r greater than the core radius, the integrals from 0 to r of the real and pseudo charge densities are in agreement; moreover, for radii greater than the core radius, the logarithmic derivatives of the real and of the pseudo wave function are identical. This also applies to their first energy derivatives.

In atoms with mean and high atomic numbers, the valence electrons are affected by relativistic effects. Therefore, Kleinman (1980) extended the concept of Hamann et al (1979) and proved that a pseudopotential for the wave function of each relativistic one-electron state can be derived for the valence electrons. These pseudopotentials satisfy the aforementioned conditions and show good transferability. In this work, the theories developed by Schlüter (1978), Hamann et al (1979), Bachelet and Schlüter (1982), Bachelet et al (1982), and Greenside and Schlüter (1983) are derived in a condensed form and, based on them, new characteristic quantities are computed. Using these characteristic quantities one is able to predict, for 1 : 1 binary intermetallic compounds and alloys, a multitude of experimental quantities and to derive systematic relations which also allow predictions to be made for mixtures that have not yet been produced.

2 Formalism

The pseudopotentials used here were derived from full-core atom calculations. For the heavier atoms, relativistic effects play a role. Therefore, the Dirac equation serves as a starting point. It is a linear matrix equation with first-order partial derivatives. The field function contains four components. For the case of a central potential, $V(r)$, the matrix equation is reduced to two coupled scalar equations. F_i and G_i represent the radial part of the minor and major components of the Dirac wave functions. Therefrom, the charge density, ρ, is computed by summing over the occupied states, i:

$$\rho(r) = \sum_i [|F_i(r)|^2 + |G_i(r)|^2]. \tag{1}$$

In place of the Schrödinger equation, the aforementioned two equations hold for the relativistic case:

$$\frac{dF_i(r)}{dr} - \frac{n}{r}F_i(r) + [\varepsilon_i - V(r)]\alpha G_i(r) = 0, \tag{2}$$

$$\frac{dG_i(r)}{dr} + \frac{n}{r}G_i(r) - \left[\frac{2}{\alpha^2} + \varepsilon_i - V(r)\right]\alpha F_i(r) = 0, \tag{3}$$

where n is the relativistic quantum number [$n = l$ for $j = l-\frac{1}{2}$, and $n = -(l+1)$ for $j = l+\frac{1}{2}$], l is the angular momentum quantum number, ε_i is an eigenvalue, and α is defined by equation (4). Here, atomic units are used and, thus,

$$c = \alpha^{-1} = 137.037 \quad \text{and} \quad \hbar = m = e = 1, \tag{4}$$

where c is the speed of light in vacuum, $\hbar$ is the Planck constant, m is the electron rest mass, and e is the electronic charge. The two different j values express that the orbital angular momentum and the spin are coupled for each electron. This then results in the splitting of the pseudopotentials. This splitting becomes visible, in particular, with the heavier atoms. The following expression is obtained for the ground-state energy:

$$E(\rho) = T(\rho) + \frac{1}{2}\int\int \frac{\rho(r)\rho(r')}{|r-r'|}\,dr\,dr' - \int \frac{Z}{r}\rho(r)\,dr + \int \rho\varepsilon_{xc}(\rho)\,dr. \tag{5}$$

The first term on the right-hand side is the kinetic energy of the electrons, the second term is the electrostatic energy of the electrons, and $-Z/r$ is the potential of the nuclei. ε_{xc} is the exchange-correlation energy per electron. After Ceperley and Alder (1980),

$$\varepsilon_x = -\frac{0.4582}{r_s} \tag{6}$$

is used for the exchange energy per electron, and

$$\varepsilon_c = -\frac{0.1432}{(1 + 1.0529r_s^{1/2} + 0.3334r_s)} \quad \text{for} \quad r_s \geq 1, \tag{7}$$

and

$$\varepsilon_c = -0.0480 + 0.0311\ln r_s - 0.0116r_s + 0.0020r_s \ln r_s \quad \text{for} \quad r_s < 1 \tag{8}$$

for the correlation energy per electron, with

$$\rho^{-1} = \frac{4\pi}{3}r_s^3. \tag{9}$$

With the help of these interpolation formulas, the exchange-correlation energy can be determined from the electron density. To allow for relativistic corrections, the exchange energy ε_x per electron has to be multiplied by a factor f_ε where

$$f_\varepsilon = 1 - \frac{3}{2}\left\{\frac{(1+\beta)^{1/2}}{\beta} - \frac{\ln[\beta + (1+\beta^2)^{1/2}]}{\beta^2}\right\}^2. \tag{10}$$

with $\beta = 0.0140/r_s$.

The exchange-correlation potential is

$$\mu_{xc}(r) = \frac{d}{d\rho}[\rho\varepsilon_{xc}(\rho)] = \varepsilon_{xc} - \frac{r_s}{3}\frac{d\varepsilon_{xc}}{dr_s}. \tag{11}$$

On the other hand, the potential μ_x has to be multiplied by f_μ, where

$$f_\mu = -\frac{1}{2} + \frac{3}{2}\frac{\ln[\beta + (1+\beta^2)^{1/2}]}{\beta(1+\beta^2)}. \tag{12}$$

Norm-conserving pseudopotentials with optimum transferability have been used here. They result from the solution of a Schrödinger-type equation:

$$\frac{1}{2}\left[\frac{d^2G_n}{dr^2}-\frac{n(n+1)}{r^2}G_n\right]-[V(r)-\varepsilon]G_n=0. \tag{13}$$

Except for higher-order quantities, this equation corresponds to the Dirac equations. The first result obtained is the radial wave function G_n, the next one F_n, and then a set of one-electron eigenvalues. By multiplication with a cut-off function $1-f$, where $f(r/r_{cj}) = \exp[-(r/r_{cj})^{3.5}]$, the singularity in the proximity of $r \approx 0$ is avoided, and a first step pseudopotential is achieved. As next steps, one has normalisation and the transition to screened pseudopotentials, producing the nodeless eigenfunctions. A last step in the calculation serves to linearise the exchange-correlation energy as a function of ρ.

The pseudopotentials defined in this way now form the starting point for the computer programs developed for this work. No matter whether one uses the initial quantities α_1, α_2, α_3, C_1, C_2, C_3, C_4, C_5, C_6 from Bachelet et al (1982) or calculates them anew, the following computing scheme suggests itself. At first, one calculates the 21 elements of the symmetrical overlap matrix, S_{il}. The following integral serves several purposes:

$$S_{ilm}=\int_0^m r^{2+\kappa}\exp[-(\alpha_i+\alpha_l)r^2]dr. \tag{14}$$

A special case is the error integral

$$\operatorname{erf} m=\frac{2}{\pi^{1/2}}S_{ilm}, \tag{15}$$

with $\kappa = -2$, $\alpha_i = 0$, and $\alpha_l = 1$. If, however, we have $\alpha_i = \alpha_{i+3}$ ($i = 1, 2, 3$) and $\alpha_l = \alpha_{l+3}$ ($l = 1, 2, 3$) and if, moreover, the following three relationships [(17), (18), (19)] apply, then the overlap matrix has to be calculated from

$$S_{il}=\lim_{m\to\infty}S_{ilm}, \tag{16}$$

where, of course, $S_{il} = S_{li}$.

$$\kappa = 0 \text{ if } i\in\{1,2,3\} \text{ and } l\in\{1,2,3\}; \tag{17}$$

$$\kappa = 4 \text{ if } i\in\{4,5,6\} \text{ and } l\in\{4,5,6\}; \tag{18}$$

$$\kappa = 2 \text{ if } i\in\{1,2,3\} \text{ and } l\in\{4,5,6\}, \text{ or } i\in\{4,5,6\} \text{ and } l\in\{1,2,3\}. \tag{19}$$

The orthogonality matrix, Q_{il}, is calculated by means of the following equations (20) from the overlap matrix:

$$Q_{11} = (S_{11})^{1/2},\quad Q_{12} = S_{12}/Q_{11},\quad Q_{13} = S_{13}/Q_{11},$$

$$Q_{14} = S_{14}/Q_{11},\quad Q_{15} = S_{15}/Q_{11},\quad Q_{16} = S_{16}/Q_{11},$$

$$Q_{22} = (S_{22}-Q_{12}^2)^{1/2},\quad Q_{23} = (S_{23}-Q_{12}Q_{13})/Q_{22},$$

$$Q_{24} = (S_{24}-Q_{12}Q_{14})/Q_{22},\quad Q_{25} = (S_{25}-Q_{12}Q_{15})/Q_{22},$$

$$Q_{26} = (S_{26}-Q_{12}Q_{16})/Q_{22},\quad Q_{33} = (S_{33}-Q_{13}^2-Q_{23}^2)^{1/2},$$

$$Q_{34} = (S_{34}-Q_{13}Q_{14}-Q_{23}Q_{24})/Q_{33},$$

$$Q_{35} = (S_{35}-Q_{13}Q_{15}-Q_{23}Q_{25})/Q_{33},$$

$$Q_{36} = (S_{36}-Q_{13}Q_{16}-Q_{23}Q_{26})/Q_{33},$$

$$Q_{44} = (S_{44}-Q_{14}^2-Q_{24}^2-Q_{34}^2)^{1/2},$$

equations (20) continued

$$Q_{45} = (S_{45} - Q_{14}Q_{15} - Q_{24}Q_{25} - Q_{34}Q_{35})/Q_{44},$$
$$Q_{46} = (S_{46} - Q_{14}Q_{16} - Q_{24}Q_{26} - Q_{34}Q_{36})/Q_{44},$$
$$Q_{55} = (S_{55} - Q_{15}^2 - Q_{25}^2 - Q_{35}^2 - Q_{45}^2)^{1/2},$$
$$Q_{56} = (S_{56} - Q_{15}Q_{16} - Q_{25}Q_{26} - Q_{35}Q_{36} - Q_{45}Q_{46})/Q_{55},$$
$$Q_{66} = (S_{66} - Q_{16}^2 - Q_{26}^2 - Q_{36}^2 - Q_{46}^2 - Q_{56}^2)^{1/2},$$
$$Q_{il} = 0 \quad \text{for } i > l. \tag{20}$$

The average pseudopotential is

$$\hat{V}_l^{\text{ion}} = \hat{V}_{\text{core}}(r) + \Delta\hat{V}_l^{\text{ion}}(r). \tag{21}$$

The short-range l-dependent part of this pseudopotential is

$$\Delta\hat{V}_l^{\text{ion}}(r) = \sum_{i=1}^{3}(A_i + r^2 A_{i+3})\exp(-\alpha_i r^2), \tag{22}$$

where the coefficients A_i are calculated as follows from C_1, ..., C_6 and Q_{il}:

$$A_6 = -C_6/Q_{66}, \tag{23a}$$
$$A_5 = -(C_5 + Q_{56}A_6)/Q_{55}, \tag{23b}$$
$$A_4 = -(C_4 + Q_{45}A_5 + Q_{46}A_6)/Q_{44}, \tag{23c}$$
$$A_3 = -(C_3 + Q_{34}A_4 + Q_{35}A_5 + Q_{36}A_6)/Q_{33}, \tag{23d}$$
$$A_2 = -(C_2 + Q_{23}A_3 + Q_{24}A_4 + Q_{25}A_5 + Q_{26}A_6)/Q_{22}, \tag{23e}$$
$$A_1 = -(C_1 + Q_{12}A_2 + Q_{13}A_3 + Q_{14}A_4 + Q_{15}A_5 + Q_{16}A_6)/Q_{11}. \tag{23f}$$

The equations given above have to be individually calculated for each chemical element and for each angular momentum quantum number l.

$$\hat{V}_{\text{core}}(r) = -\frac{Z_v}{r}\sum_{j=1}^{2} C_j^{\text{core}}\,\text{erf}[(\alpha_j^{\text{core}})^{1/2}r], \tag{24}$$

where Z_v is the valence charge.

Now, based on the pseudopotential $\hat{V}_l^{\text{ion}}$ that can be calculated in this manner, one can pursue two lines of thought which are of importance for the question of the chemical composition of the Earth's outer and inner cores. First, using an approach that is similar to that adopted by Ihm et al (1979), one can calculate from it the total energy for one substance. From the total energy it is possible—in a manner similar to Walzer (1987a, 1987b)—to determine the equation of state, the bulk modulus, and other variables; and to compare them with experimental values from physical laboratories. When a physically verifiable model has been established, it can be applied to geochemical hypotheses for the chemical composition of the outer core of the earth, and one can examine whether the computed distributions of the mass density and of the seismic velocities conform, within the error limits, with the geophysically measured distributions. When doing so, one would make an implicit assumption that is common in geophysics, but which is not precisely true: that under pressure, the phase diagram of binary mixtures should be compressed or extended only in the temperature direction, but not significantly altered (eg through the appearance or disappearance of certain phases).

Second, one may attempt to determine characteristic quantities from the potentials in order to find the systematics of binary intermetallic compounds and alloys.

In contrast to compounds, one can continually change the mixture ratios in the case of alloys. For reasons of simplicity, this paper is confined to binary 1 : 1 mixtures. However, the method used is by no means limited to this ratio. The determination of systematic distributions has the advantage that properties can be predicted for material mixtures of this kind that have not yet been produced. If, for practical reasons, certain properties are desirable, one could confine oneself to the production of those compounds which have a theoretically favourable location in the present plots. In the present paper, I wish to pursue the second line, which may also make a certain contribution to the determination of the chemical composition of the Earth's core.

The influence of the spin–orbit effects on the pseudopotential is described by

$$\hat{V}_l^{\mathrm{so}}(r) = \left[\frac{2}{2l+1}\right](\hat{V}_{l+1/2}^{\mathrm{ion}} - \hat{V}_{l-1/2}^{\mathrm{ion}}). \tag{25}$$

The average pseudopotential introduced through equation (21) can be expressed as follows by means of the different j degeneracies of the $l \pm \frac{1}{2}$ states:

$$\hat{V}_l^{\mathrm{ion}}(r) = \left[\frac{1}{2l+1}\right][l\hat{V}_{l-1/2}^{\mathrm{ion}} + (l+1)\hat{V}_{l+1/2}^{\mathrm{ion}}]. \tag{26}$$

From this expression, there follow equations (27) and (28):

$$\hat{V}_{l-1/2}^{\mathrm{ion}}(r) = \hat{V}_l^{\mathrm{ion}}(r) - \frac{(l+1)}{2}\hat{V}_l^{\mathrm{so}}(r), \tag{27}$$

$$\hat{V}_{l+1/2}^{\mathrm{ion}}(r) = \hat{V}_l^{\mathrm{ion}}(r) + \frac{l}{2}\hat{V}_l^{\mathrm{so}}(r). \tag{28}$$

Now, one calculates the bare-ion pseudopotentials $\hat{V}_{l\pm1/2}^{\mathrm{ion}}$ as a function of the distance, r, from the centre of the atom. These curves show minima and locations of maximum curvature. For these special radii or for physically useful functions of the same, one may form, for instance, structure maps for a given stoichiometry, eg AB, and check whether systematic distributions develop. As far as this was possible, the following variables were determined for the elements hydrogen to plutonium:

$$r_{\mathrm{m}0}, \upsilon_{\mathrm{m}0}, e_{\mathrm{m}0};\ r_{\mathrm{m}1}, \upsilon_{\mathrm{m}1}, e_{\mathrm{m}1};\ r_{\mathrm{p}1}, \upsilon_{\mathrm{p}1}, e_{\mathrm{p}1};$$

$$r_{\mathrm{m}2}, \upsilon_{\mathrm{m}2}, e_{\mathrm{m}2};\ r_{\mathrm{p}2}, \upsilon_{\mathrm{p}2}, e_{\mathrm{p}2};\ r_{\mathrm{m}3}, \upsilon_{\mathrm{m}3}, e_{\mathrm{m}3}. \tag{29}$$

The number triples are separated by semicolons. r and υ are, respectively, the radius and the pseudopotential of the characteristic point. e is the genuineness. If $e = 1$, the pertaining r and υ denote, respectively, the radius and potential of the first minimum which is reached coming from infinite r; both are expressed in atomic units. If this minimum is situated at the origin of r, we assume that $e = 0$; and the number pair (r, υ) is substituted by the location with the greatest curvature of the curve. Subscript m means minus and relates to the pseudopotential of equation (27); subscript p means plus and related to equation (28). The indices 0–3 denote the angular momentum quantum number l used in (27) and (28). In more precise terms, $e = 0$ means that υ is at its minimum for $r = 0$. The listed number pair (r, υ) then designates the location of the curve where at the same time we have $\mathrm{d}^2\upsilon/\mathrm{d}r^2 > 0$, and curvature k coming from the infinitely large r reaches a maximum, with

$$k = \frac{\mathrm{d}^2\upsilon}{\mathrm{d}r^2}\left[1 + \left(\frac{\mathrm{d}\upsilon}{\mathrm{d}r}\right)^2\right]^{-3/2}. \tag{30}$$

To define further characteristic quantities from the pseudopotentials calculated, an additional index is attached to the quantities listed in (29). This index denotes the

atomic species, and can be 1 or 2 in the case of a binary mixture. Thus, for example, r_{p12} is the radius of the minimum (or, in the special case, point of maximum curvature) in atomic units according to formula (28) for $l = 1$ and for the second atomic species in a binary 1 : 1 mixture. A kind of size difference may be defined as

$$R_\sigma^{(w)} = |(r_{11}+r_{m01})-(r_{12}+r_{m02})|, \tag{31}$$

where

$$r_{11} = \tfrac{1}{2}(r_{m11}+r_{p11}) \quad \text{and} \quad r_{12} = \tfrac{1}{2}(r_{m12}+r_{p12}). \tag{32}$$

Moreover, $R_\pi^{(w)}$ is defined as

$$R_\pi^{(w)} = |r_{11}-r_{m01}|+|r_{12}-r_{m02}|, \tag{33}$$

and is a function of hybridisation.

3 Numerical results

The author has developed new computer programs on the basis of the theory outlined above. In figures 1a–1e, a few pseudopotentials have been plotted as examples for the elements from hydrogen to plutonium. They have been calculated according to equations (27) and (28). For boron, the relativistic effect is not yet visible. For sulphur, one finds a bifurcation in the curve for $l = 1$; this bifurcation can be represented only as a thickening of lines. With niobium and indium, two curves are already well visible for $l = 1$ and $l = 2$; whereas for mercury—the heaviest of the elements represented here—the distance between $\hat{V}^{ion}_{l-1/2}$ (left-hand) and $\hat{V}^{ion}_{l+1/2}$ (right-hand) is already quite large. It should be noted here that—for the purpose of illustrating the quantities listed in (29)—in figure 1a (boron), for example, the points (r_{m0}, v_{m0}), (r_{m1}, v_{m1}), and (r_{m2}, v_{m2}) have been represented by the intersections of the short strokes in the proximity of the numbers $l = 0$, 1, and 2.

Figures 2–10, too, have been plotted by means of the computer. The symbols are defined in table 1. The theoretical values have all been obtained with the help of the theory considered in section 2. The quantities observed have all been taken from the encyclopaedia of Villars and Calvert (1985). Values were neither added nor omitted so that the results given are objective. Figure 2 shows that, in a $R_\pi^{(w)}$ versus $R_\sigma^{(w)}$ plot for all known 1 : 1 mixtures, the three most frequent crystal lattices do not show a random distribution. On the contrary, fields can be separated from one another in which one type of lattice is prevailing. In figure 3, it is shown in the plot for the radii and pseudopotentials related to $l = 2$ that the compounds and alloys consisting only of transition metals (TT) aggregate in a small area of the left-hand centre of the plot;

Table 1. The assignment of symbols for the plots in which the symbols express the space group of the crystal lattice.

Space group	Structure type	Symbol	Space group	Structure type	Symbol
$Fm\bar{3}m$	ClNa	■	Pnma	BFe	▼
$Fm\bar{3}m$	Cu	□	Pnma	MnP	▲
$F\bar{4}3m$	SZn	○	P4/mmm	AuCu	◀
$Fd\bar{3}m$	NaTl	∧	P4/nmm	CuTi	▶
$Pm\bar{3}m$	ClCs	◆	$P\bar{4}3n$	GeK	<
$P6_3/mmc$	AsNi	●	$P2_13$	FeSi	>
$P6_3/mmc$	Mg	◇	Cmcm	BCr	+
$P6_3mc$	SZn	∨	$Im\bar{3}m$	W	×
			$I4_1/acd$	NaPb	*

the remaining ones are situated on a few lines for still smaller mean radii. The compounds and alloys consisting only of simple metals (SS) prevail in the zone with small negative potentials and large radii. In the middle, one finds only compounds consisting of simple metals and transition metals (ST). In the upper centre, ST and SS intermingle. Figure 4 shows a similar distribution of points as figure 3, but radii and pseudopotentials apply to $l = 0$. The first thing that is noticed is that the characteristic shows less scattering. The symbols of figure 4 represent the crystal lattices. Weakly curved curves of identical lattice symbols prevail. Owing to the density of the point cloud, this is noticeable here only at the edges of the cloud, but it is also applicable to its interior. In figure 5, the lattice symbols are plotted only for TT in a radius–pseudopotential diagram. Radii and potentials relate to $l = 0$.

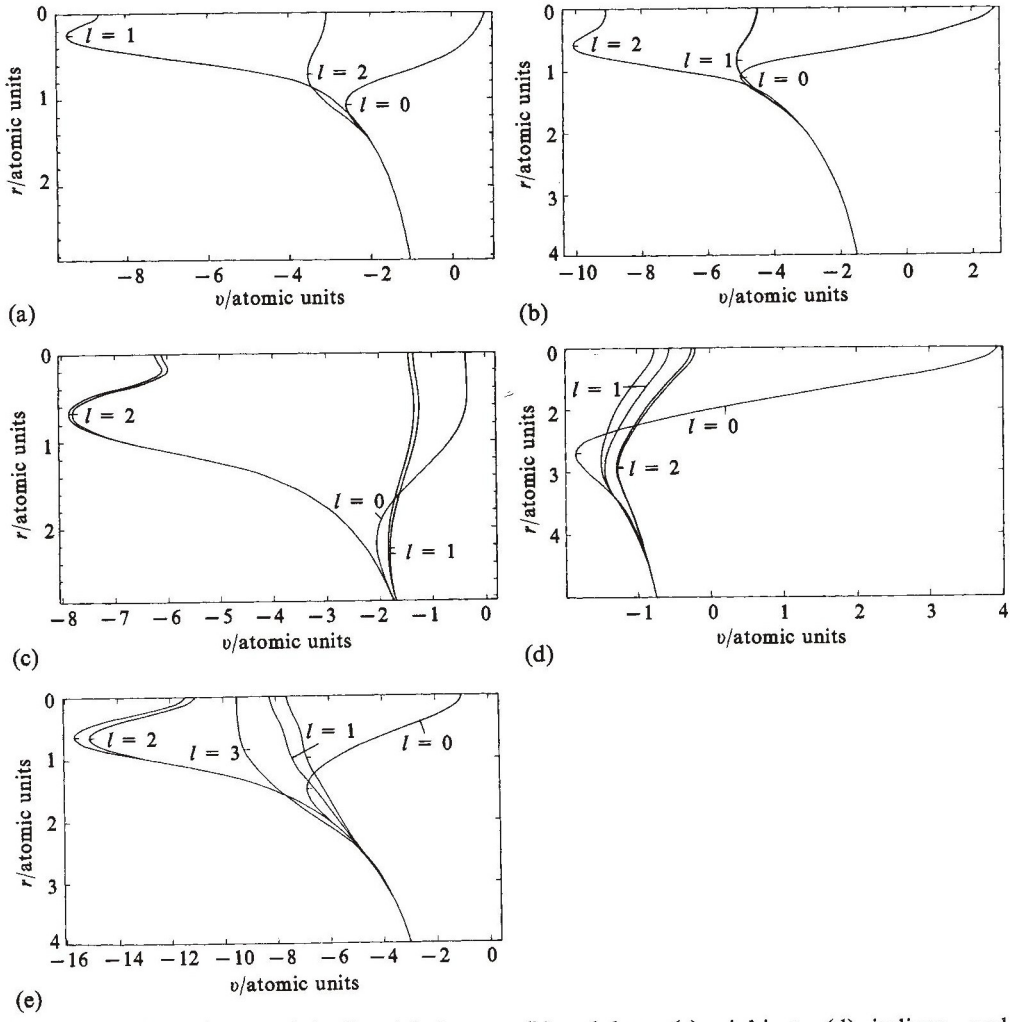

Figure 1. Pseudopotentials for (a) boron, (b) sulphur, (c) niobium, (d) indium, and (e) mercury, according to equations (27) and (28). The distance r, from the centre of the atom is plotted downwards, and the pseudopotential, υ, is plotted towards the right; both are in atomic units. The angular momentum quantum number, l, according to equation (27) is written on the curves. The minima or points of maximum curvature (for more details, see text) are marked by short strokes on the curves. They have also been calculated by means of the computer program.

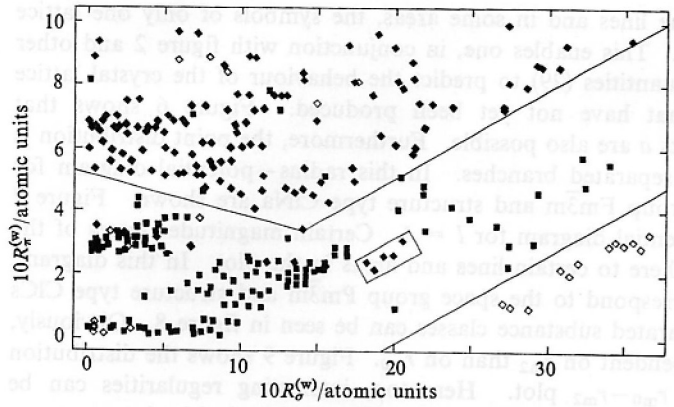

Figure 2. Crystal lattice as a function of $R_\sigma^{(w)}$ and $R_\pi^{(w)}$ (both in atomic units). Full diamonds denote lattices with space group $Pm\bar{3}m$ and structure type ClCs, full squares for space group $Fm\bar{3}m$ and structure type ClNa, open diamonds for lattices with space group $P6_3/mmc$ and structure type Mg. The oblique straight lines denote the separation between the crystal lattices.

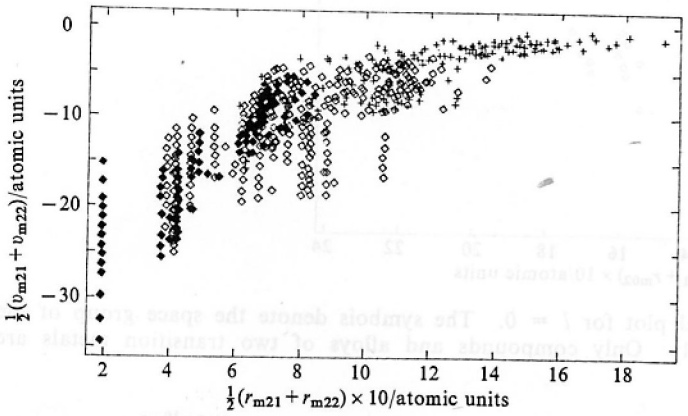

Figure 3. Radius–potential diagram for $l = 2$. Solid diamonds represent compounds and alloys of two transition metals, open diamonds represent those of a transition metal and a simple metal, crosses represent compounds or alloys of two simple metals.

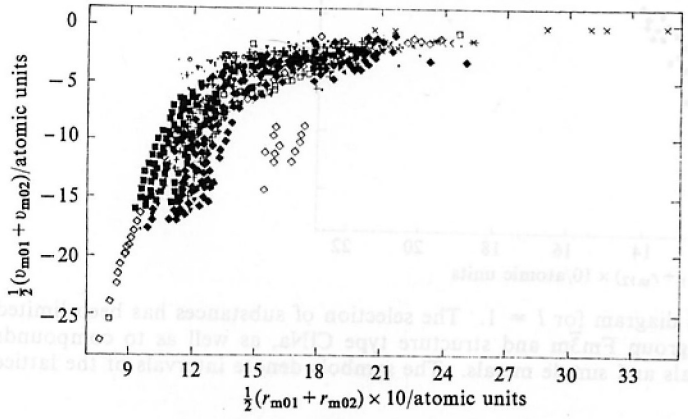

Figure 4. Radius–potential plot for $l = 0$. The symbols express the space group of the crystal lattice; see table 1.

It can be seen that on some lines and in some areas, the symbols of only one lattice type are present or prevailing. This enables one, in conjunction with figure 2 and other plots, to use the theoretical quantities (29) to predict the behaviour of the crystal lattice of compounds and alloys that have not yet been produced. Figure 6 shows that predictions for lattice constants a are also possible. Furthermore, the point distribution is characterised by four clearly separated branches. In this radius–potential diagram for $l = 1$, only ST with space group $Fm\bar{3}m$ and structure type ClNa are shown. Figure 7 contains a radius–pseudopotential diagram for $l = 1$. Certain magnitude classes of the lattice constants a are linked here to certain lines and areas in the plot. In this diagram, only ST with lattices that correspond to the space group $Pm\bar{3}m$ and structure type ClCs are plotted. Two clearly separated substance classes can be seen in figure 8. Obviously, lattice constant a is more dependent on r_{m2} than on r_{m0}. Figure 9 shows the distribution of TT, SS, and ST in the $r_{m0}-r_{m2}$ plot. Here too, interesting regularities can be observed. Finally, figure 10 shows a clear division into areas of identical lattice types.

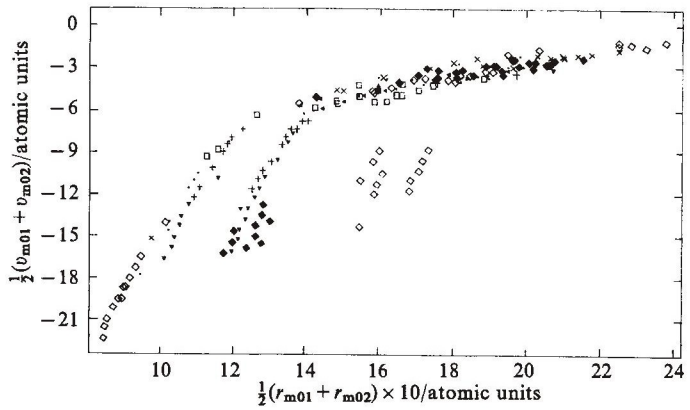

Figure 5. Radius–potential plot for $l = 0$. The symbols denote the space group of the crystal lattice; see table 1. Only compounds and alloys of two transition metals are represented.

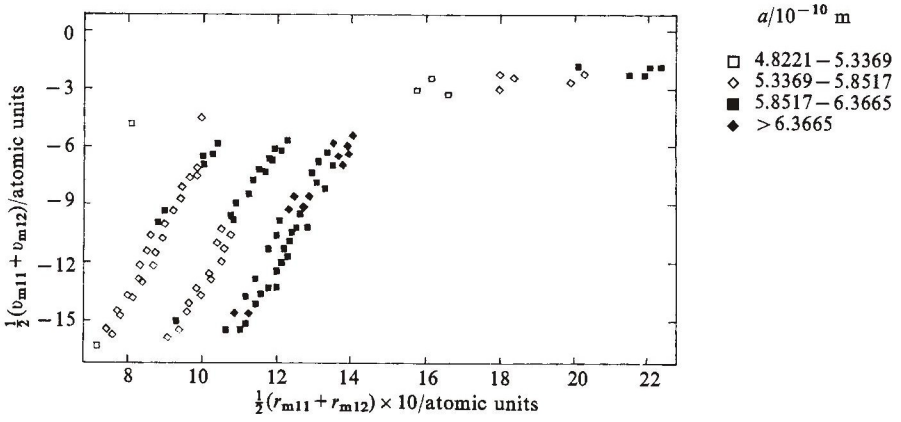

Figure 6. Radius–potential diagram for $l = 1$. The selection of substances has been limited here to crystals with space group $Fm\bar{3}m$ and structure type ClNa, as well as to compounds and alloys of transition metals and simple metals. The symbols denote intervals of the lattice constants a.

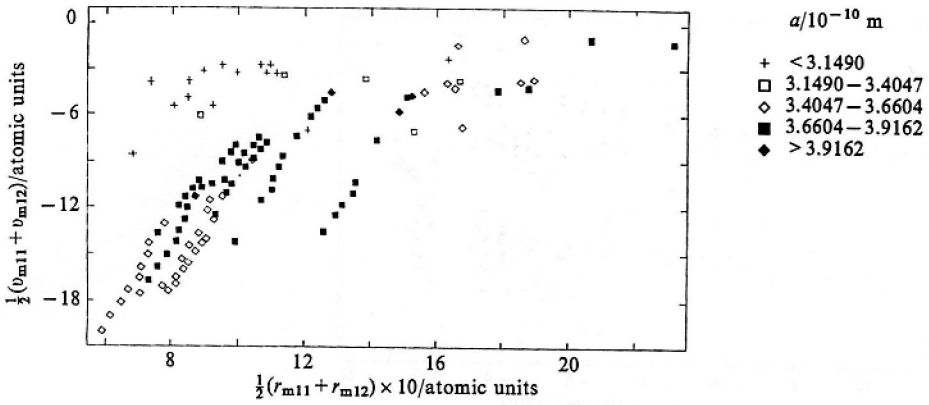

Figure 7. Radius−potential plot for $l = 1$. Here, only transition-metal−simple-metal compounds which are present in crystals with space group $Pm\bar{3}m$ and structure type ClCs are represented. The symbols designate intervals of the lattice constants a.

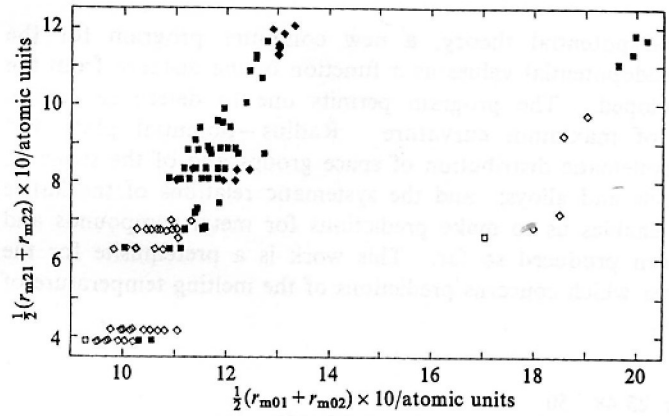

Figure 8. Radius−radius diagram. The selection of substances is limited here to transition-metal−simple-metal compounds, the crystals of which have space group $Fm\bar{3}m$ and structure type ClNa. For symbols and interval arrangement depending on the magnitude of the lattice constants a, see figure 6.

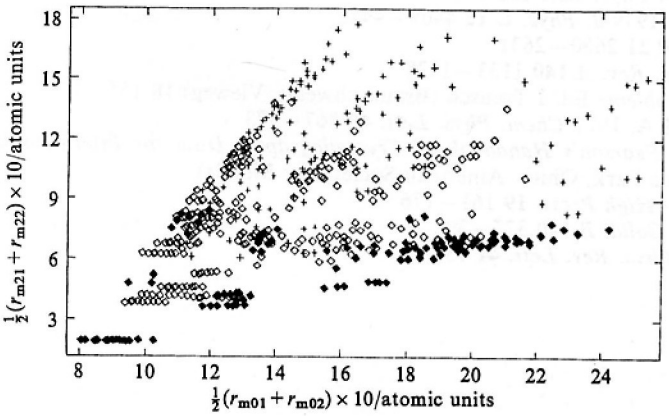

Figure 9. Radius−radius plot. Solid diamonds represent compounds and alloys of two transition metals, open diamonds represent those of a transition metal and a simple metal. Crosses stand for compounds and alloys of two simple metals.

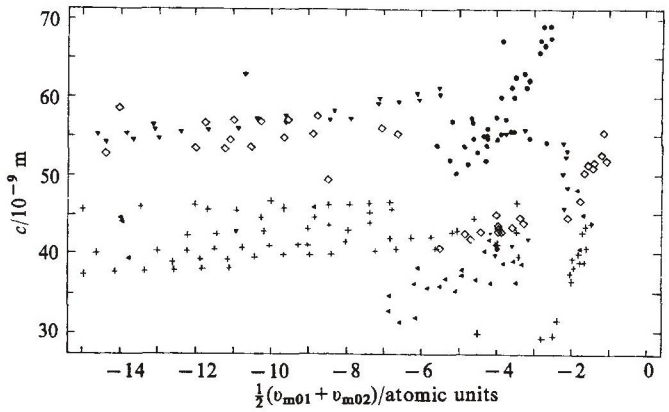

Figure 10. Potential–lattice constant plot. The symbols are explained in table 1 and denote the space group and structure type of the crystals.

4 Conclusions

Based on an extended pseudopotential theory, a new computer program for the calculation of *l*-dependent pseudopotential values as a function of the distance from the atomic centre has been developed. The program permits one to determine certain extreme values and points of maximum curvature. Radius–potential plots and radius–radius plots show a systematic distribution of space groups and of the structure types of binary 1:1 compounds and alloys; and the systematic relations of the lattice constants *a*, *b*, and *c*. This enables us to make predictions for metal compounds and alloys which have not yet been produced so far. This work is a prerequisite for the understanding of a future paper which concerns predictions of the melting temperature of the substances considered here.

References

Ashcroft N W, 1966 *Phys. Lett.* **23** 48–50
Bachelet G B, Hamann D R, Schlüter M, 1982 *Phys. Rev. B* **26** 4199–4228
Bachelet G B, Schlüter M, 1982 *Phys. Rev. B* **25** 2103–2108
Ceperley D M, Alder B J, 1980 *Phys. Rev. Lett.* **45** 566–569
Greenside H S, Schlüter M, 1983 *Phys. Rev. B* **28** 535–543
Hamann D R, Schlüter M, Chiang C, 1979 *Phys. Rev. Lett.* **43** 1494–1497
Hohenberg P C, Kohn W, 1964 *Phys. Rev.* **136** 864–871
Ihm J, Zunger A, Cohen M L, 1979 *J. Phys. C* **12** 4409–4422
Kleinman L, 1980 *Phys. Rev. B* **21** 2630–2631
Kohn W, Sham L J, 1965 *Phys. Rev. A* **140** 1133–1138
Schlüter M, 1978 *Festkörperprobleme* Ed. I Treusch (Braunschweig: Vieweg) **18** 155–191
Topiol S, Zunger A, Ratner M A, 1977 *Chem. Phys. Lett.* **49** 367–373
Villars P, Calvert L D, 1985 *Pearson's Handbook of Crystallographic Data for Intermetallic Phases* volumes 1–3 (Metals Park, Ohio: American Society for Metals)
Walzer U, 1987a *High Temp.–High Press.* **19** 161–176
Walzer U, 1987b *Phys. Status Solidi B* **140** 377–391
Zunger A, Cohen M L, 1978 *Phys. Rev. Lett.* **41** 53–56